photochem

MDPI

Article

Theoretical Modeling of Absorption and Fluorescent Characteristics of Cyanine Dyes

Sonia Ilieva, Meglena Kandinska, Aleksey Vasilev and Diana Cheshmedzhieva *

Faculty of Chemistry and Pharmacy, Sofia University "St. Kliment Ohridski", 1164 Sofia, Bulgaria; silieva@chem.uni-sofia.bg (S.I.); ohmk@chem.uni-sofia.bg (M.K.); ohtavv@chem.uni-sofia.bg (A.V.)
* Correspondence: dvalentinova@chem.uni-sofia.bg; Tel.: +359-28161354

Abstract: The rational design of cyanine dyes for the fine-tuning of their photophysical properties undoubtedly requires theoretical considerations for understanding and predicting their absorption and fluorescence characteristics. The present study aims to assess the applicability and accuracy of several DFT functionals for calculating the absorption and fluorescence maxima of monomethine cyanine dyes. Ten DFT functionals and different basis sets were examined to select the proper theoretical model for calculating the electronic transitions of eight representative molecules from this class of compounds. The self-aggregation of the dyes was also considered. The pure exchange functionals (M06L, HFS, HFB, B97D) combined with the triple-zeta basis set 6-311+G(2d,p) showed the best performance during the theoretical estimation of the absorption and fluorescent characteristics of cyanine dyes.

Keywords: cyanine dyes; DFT; TDDFT; UV-VIS spectroscopy; fluorescence; aggregation; dimers; DNA

check for updates

Citation: Ilieva, S.; Kandinska, M.; Vasilev, A.; Cheshmedzhieva, D. Theoretical Modeling of Absorption and Fluorescent Characteristics of Cyanine Dyes. *Photochem* **2022**, *2*, 202–216. https://doi.org/10.3390/photochem2010015

Academic Editors: Gulce Ogruc Ildiz and Licinia L.G. Justino

Received: 20 December 2021
Accepted: 1 March 2022
Published: 4 March 2022

Publisher's Note: MDPI stays neutral with regard to jurisdictional claims in published maps and institutional affiliations.

Copyright: © 2022 by the authors. Licensee MDPI, Basel, Switzerland. This article is an open access article distributed under the terms and conditions of the Creative Commons Attribution (CC BY) license (https://creativecommons.org/licenses/by/4.0/).

1. Introduction

Fluorescent dyes are widely used for the detection and quantification of nucleic acids (NA) and proteins and are applied in real-time PCR, gel electrophoresis, flow cytometry, microscopy, etc. [1–3]. This is due to the ability of specific fluorescent dyes to bind to various target biomolecules in a mostly noncovalent mode, leading to changes in the fluorescent properties of the respective dye. Any significant changes in the photophysical properties of the dye would be useful, but the most used one is the increase in the emission intensity of the dye upon binding. Cyanine dyes are a wide class of cationic compounds that have been proven to be efficient probes for nucleic acid detection [4] due to the fact that they have very low fluorescence intensity before binding, and this intensity increases significantly after binding to NA. Two types of nucleic acid binding have been demonstrated for these compounds: intercalation and minor groove binding [5–9]. Cyanine dyes are known to extend over the visible and near infrared spectrum due to changes in the length of the central polymethine bridge or the heterocycles [4,10]. The dye spectrum can be fine-tuned by introducing substituents into the aromatic heterocycles [11]. Because of their importance as fluorogenic acid probes, the cyanines have been the subject of versatile research in the last decade [7,11–18]. The development of new fluorescent probes for dsRNA is even more important nowadays [18,19]. The broad application of cyanine dyes in medicine and diagnostics [20–23] fuels the interest in them. The rational design of new functional materials requires a deep understanding of the driving forces behind the changes in the photophysical properties of the synthesized dyes as well as the binding mode toward the biomolecular targets. The rational approach to that problem requires a body of knowledge about the properties of the dye itself and the changes that these properties undergo upon binding. Undoubtedly, this knowledge includes experimental synthetic and spectroscopic studies as well as theoretical considerations of the dyes' properties for resolving the factors governing the binding and selectivity towards nucleic acids. Quantum chemical computations provide information that allow us to have a deeper understanding of the binding

to the DNA mechanism, structure of the ligands and complexes, and photochemical and spectral characteristics of the dyes [11,14,24–28].

The present study aims to assess the applicability and accuracy of several DFT functionals for calculating the absorption and fluorescent maxima of monomethine cyanine dyes. It is generally accepted that DFT provides adequate description of the geometry and physico-chemical properties of organic compounds in their ground state [29]. Time-Dependent Density Functional Theory (TDDFT) formalism is considered to be an adequate and robust tool for the computation of the electronic structure and geometry in the excited state for various organic compounds [14,30,31]. In some earlier studies, the TDDFT approach was considered to have poor performance when studying the photophysical properties of cyanines due to the overstimulation of the electron transition energies for this class of compounds [11,26,31–33]. It has been discussed that TDDFT's poor performance in cyanines is due to the multi-reference nature of the electronic states of the dyes, especially when compared to the results of the CASPT2 method [34,35]. The applicability of the TDDFT approach for characterizing cyanine dyes has recently been reconsidered [14,24]. A comparison between the performance and accuracy of several Minnesota and PBE functionals with respect to Quantum Monte Carlo and CASPT2 calculations for cyanines is published from D. Truhlar and co-authors [14]. The work of Send et al. [24] also recognizes TDDFT by considering the electronic excitation of simple cyanine dyes compared to QMC, CASPT2, and the coupled cluster method (up to CC3). A conclusion was drawn that TDDFT is an adequate and reliable tool for the calculation of the excited-state electronic structures of organic molecules [32,36], including the class of cyanine dyes [14]. The combination of the functional and the basis set within the TDDFT method must be chosen for the specific fluorophore carefully. Thus, based on the already settled important issue that TDDFT does not show any shortcomings in the resolution of cyanine functionality, the aim of the present study concerns the TDDFT applications for a specific class of cyanines with more complex structure. The objective is to find functional-basis set combinations that are suitable for describing the specific chromophore for a group of monomethinecyanine dyes that are studied. We examined ten DFT functionals and different basis sets to select the proper theoretical model for calculating the electronic transitions of cyanine dyes. The theoretical results were validated against experimental data for the dyes studied.

2. Computational Methods

Quantum chemical computations were applied to simulate the geometry, electronic structure, and spectral properties for a series of cyanine dyes.

The geometry optimization and photophysical properties of the monomers of thiazole orange (TO) and the seven analogues that were studied were computed using the G16 software package [37]. The minimum energy structures in the ground state were optimized at the DFT [38] theory level using the B3LYP hybrid function in conjunction with the 6-31G(d,p) [39] basis set, and for the iodide counterions, only the SDD basis set and effective core potential were used [40–43]. The plausible TO dimers were optimized at M062X/6-31G(d,p) (SDD basis set used for the iodide counterions).

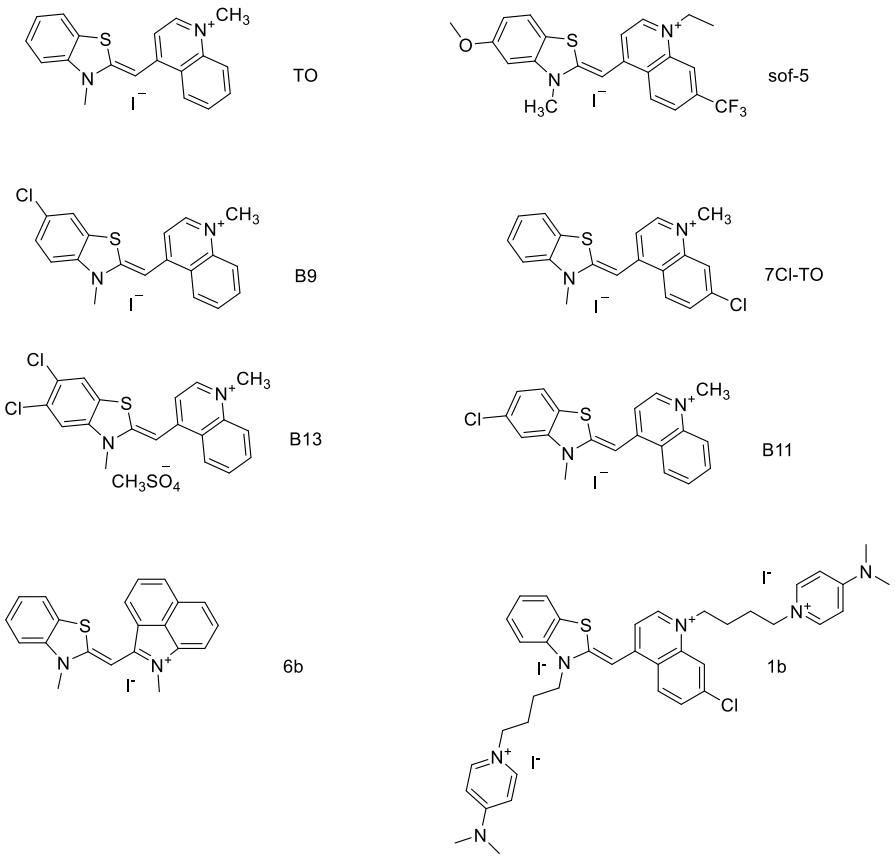
The effect of the medium was taken into account at each step by means of PCM formalism [44,45]. All of the computations were performed in a water medium to reproduce the experimental conditions (TE buffer). In order to verify that each optimized structure is a minimum of the potential energy surface, an analysis of the harmonic vibrational frequencies was performed using the same method/basis, set and no imaginary frequency was found. To determine the absorption wavelengths, the lowest energy absorption transitions were evaluated by TDDFT calculations of the vertical excitations. Ten different functional basis sets: B3LYP [46], PBE0 [47,48], M062X, M06, M06L [49], BH and HLYP [50], CAM-B3LYP [51], HFS [52,53], HFB [54], and B97D [55] with 6-311+G(2d,p) [56], were used to assess the accuracy of the functionals in predicting the spectral properties of cyanine dyes. The procedure for vertical absorption and emission computations is described in our previous work [30]. The following steps were included in the computations: (i) geom-

etry optimization of the ground-state structure at the DFT level and the computation of vibrational frequencies using the same method/basis set to verify the optimized structure. (ii) TDDFT calculations of vertical excitations to estimate the lowest energy absorption transition. Six excited singlet states were considered, and the lowest energy transition with non-zero oscillator strength was taken into account for each of the monomer dyes from the series. Comparisons were made for two of the cyanine dyes using calculations that considered 12, 20, and 24 excited states. As a result, no significant difference in the vertical excitation energy was obtained. Twenty excited singlet states were considered for the dimer absorption spectra computations. (iii) After the excited state of interest was identified, TDDFT geometry optimization with equilibrium linear response solvation was performed. The optimization of the excited state at the TDDFT level starting from the ground state geometry was determined. Frequency calculations and the absence of imaginary frequencies confirm the equilibrium of the excited-state geometry. (iv) Fluorescence electronic transitions–TDDFT calculations of the vertical de-excitations based on the optimized geometry of the excited state. Vertical excitation and de-excitation energies were calculated without state-specific correction. The computed absorption and emission transitions in solution were compared to the experimental spectral data.

3. Results

3.1. Geometry Optimization

A series of eight asymmetric cyanine dyes (Scheme 1) were modelled with the help of DFT and TDDFT calculations to gather deep insights into the geometry and electron density distribution in the ground and excited states and to achieve a better understanding of the electronic spectra of the dyes. The cyanine dyes that were used in the present study were previously synthesized by our group [18,57,58].



Scheme 1. Thiazole orange (TO) analogues. Dye labelling is the same as in the original papers.

The geometries of the *cis*- and *trans*- TO conformers optimized at the B3LYP/6-31G(d,p) theory levels are presented in Figure 1. For all of the studied cyanine dyes, the *trans* conformer is more stable than the *cis* conformer. Geometry parameters and some spectral characteristics of several of the conformational TO states are provided in Table 1. The energy difference between the *cis* and *trans* TO conformers is 5.4 kcal/mol in favour of the trans conformer. The main difference between the two conformational states, *cis* and *trans*, is the dihedral angle between the quinoline and benzothiazole heterocycles-τ($SC_2C_4C_6$). The *cis* conformer is not planar, and the dihedral angle τ($S_1C_2C_4C_6$) is 125.7°. Due to some steric hindrance between the two heterocycles, the *trans* conformer is not fully planar. In the *trans* conformer, the angle τ($S_1C_2C_4C_6$) is 17.8°, thus leading to a conjugation between the two heterocycles through the methine bridge. These theoretical results are in agreement with the results of other conformational NMR studies [59].

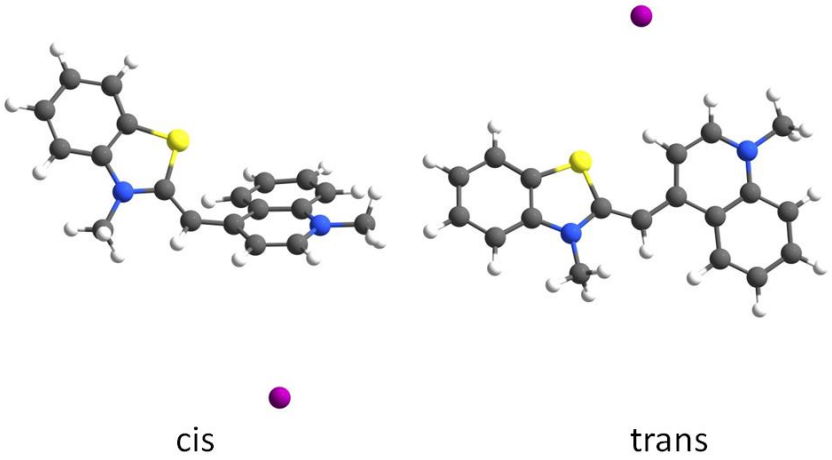
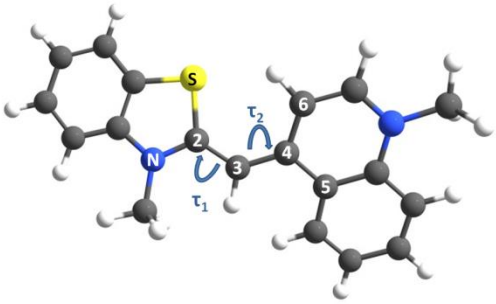


Figure 1. B3LYP/6-31G(d,p)-optimized geometry of *cis* and *trans* TO conformers. Color scheme: C–gray, S–yellow, H–white, N–blue, I–magenta.

Table 1. B3LYP/6-31G(d,p)-optimized geometry parameters, absorption maxima (nm), and oscillator strength (f) from PBE0/6-311+G(2d,p) computations for several conformational TO states.



Isomer	τ_1 (NC_2C_3H)	τ_2 ($HC_3C_4C_5$)	τ ($C_2C_3C_4C_6$)	ΔG (kcal/mol)	λ_{abs} (nm)	f
cis	−14.8	157.7	145.6	5.4	476.8	0.6706
trans	6.4	10.0	12.7	0.0	447.2	0.9598
trans 2	6.5	9.1	11.8	0.8	448.8	0.9000
trans 3	−6.5	−10.6	−13.2	1.5	447.2	0.9504

Furthermore, due to variations in the counterion position and the influence of the counterion position on some photophysical TO characteristics, different *trans* conformations were considered. The geometry parameters and spectral characteristics of three trans conformers with different counterion positions are provided in Table 1. The calculations

show that the position of the counterion has little influence on the Gibbs free energy of the conformers and their absorption maxima.

3.2. Modelling Spectroscopic Properties

Computing the molecular properties of organic compounds in the ground state is more or less systematic, while the theoretical calculation of excited state properties, such as absorption and fluorescence maxima, is not so trivial. A careful calibration of the theoretical model applied to perform computational studies for a series of molecules with a particular chromophore is of critical importance.

The absorption maxima of the dyes that were studied were computed using the B3LYP/6-31G(d,p)-optimized geometry of the molecules. Vertical excitations were obtained from single point TDDFT computations on the optimized geometries using ten different functionals: B3LYP, PBE0, M062X, M06, M06L, BH and HLYP, CAM-B3LYP, HFS, HFB, and B97D, to find an accurate description of the electronic excitations as well as to predict the absorption and emission spectral characteristics. The vertical excitations/absorption maxima were computed in the ground-state geometry. All of the computations were made in a water medium to mimic the experimental conditions. The solvent effect was modeled using the SCRF formalism IEFPCM.

TDDFT allows transition energies as well as excited-state properties such as dipole moments and emitting geometries to be computed [60,61]. Despite its huge popularity, the reliability of TDDFT results depends significantly on the selected exchange–correlation (XC) functional. The accepted accuracy of TDDFT computations is 0.2–0.3 eV [62]. The chemical accuracy of the 0.1 eV difference between the calculated and measured absorption maxima has not yet been reached.

In the literature, one of the ways to overcome this is to use range-separated hybrids (RSH) [62–65]. These functionals incorporate a growing fraction of exact exchange with increasing inter-electronic distance and allow the charge-transfer phenomena to be modelled accurately. Range-separated functionals (RSF) are a subgroup of hybrid functionals. While conventional (global) hybrid functionals such as PBE0 or B3LYP use fixed Hartree–Fock and DFT exchange, RSFs mix the two contributions based on the spatial distance between two points.

The predicted absorption wavelengths of the lowest electronic energy transitions and respective oscillator strengths for the *cis* and *trans* TO conformers are listed in the last two columns of Table 1. Vertical excitation energies computed at the PBE0/6-311+G(2d,p) level of theory without any state-specific correction are reported in Table 1. It can be seen that the calculated absorption maximum of the *cis* conformer (477 nm) is batochromicaly shifted compared to the *trans* absorption maxima (447–449 nm). The transitions of the two conformers show different oscillator strength, which is lower for the *cis* conformer.

The molecular orbitals involved in the $S_0 \rightarrow S_1$ transitions for the *cis* and *trans* conformers were calculated. Figure 2 shows the ground-state orbital energy levels of the highest occupied molecular orbital (HOMO), the lowest unoccupied molecular orbital (LUMO), and the energy gap for the *cis* TO and the *trans* TO in water. The trends in electron density change can be illustrated through the molecular orbitals shape analysis. The HOMO has a higher electron density on the benzothiazole ring. As seen from Figure 2, the electron density is redistributed from the benzothiazole and moves toward the quinoline heterocycle of the *cis* and *trans* TOs. Strong charge transfer is observed from the benzothiazole ring toward the quinoline portion, accompanying the electronic transition in the *cis* TO conformer. The strong charge transfer observed for the *cis* conformer explains the red shift of the transition. For the other compounds being studied, only the most stable conformer was considered.

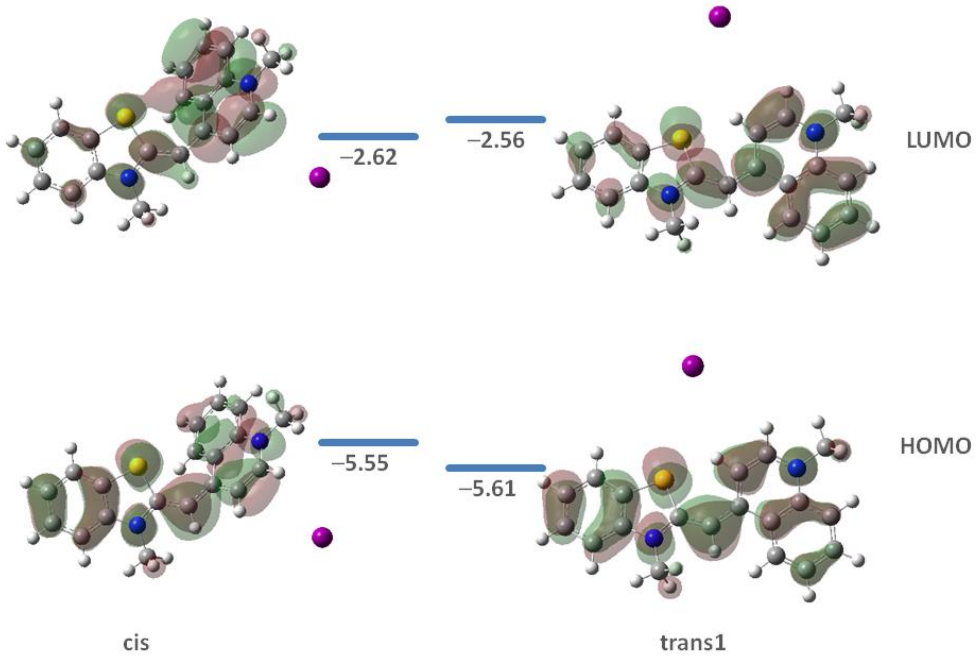


Figure 2. Molecular orbitals involved in the $S_0 \rightarrow S_1$ transition for *cis* and *trans* TO conformers computed at B3LYP/6-31G(d,p) in water medium.

The influence of the basis set on the absorption maxima calculations was considered. The theoretical vertical excitation energies were computed with six Pople-type basis sets. The results that were obtained are summarized in Table 2. As seen from Table 2, the addition of one diffuse function to the 6-31G(d,p) basis set instantly increases the value of the calculated absorption maximum, thus improving the results obtained with 6-31+G(d,p). The best results were obtained with the large 6-311+G(2d,p) basis set (2.71 eV(458 nm) the predicted maximum, 2.47 eV(502 nm)–experimental value). The difference between the theoretical estimation and the experimental value was 0.24 eV, which is an acceptable accuracy. Benchmark calculations on the absorption properties of various systems have demonstrated that the expected TDDFT accuracy is between 0.2 and 0.3 eV [30,62,66].

Table 2. Computed absorption maxima λ_{abs} (nm) for TO computed with PBE0 functional and different basis sets.

Basis Set	λ_{abs} [nm] PCM	λ_{abs} [nm] SMD
6-31G(d,p)	445	445
6-31+G(d,p)	454	453
6-31++G(d,p)	454	453
6-311G(d,p)	451	450
6-311+G(d,p)	452	455
6-311+G(2d,p)	458	457
Experiment λ_{abs} (nm)	502 [a]	

[a] From Ref. [64].

Further calculations of vertical absorptions for a series of eight cyanine dyes were carried out with different functionals combined with the triple-zeta basis set 6-311+G(2d,p). Table 3 summarizes the vertical absorption energies calculated with ten different TDDFT functionals: B3LYP, PBE0, M062X, M06, M06L, BH and HLYP, CAM-B3LYP, HFS, HFB, and B97D. The applied functionals differ in the form of their exchange functional. This functional has various percentage HF exchange (0% to 54%). A comparison between the theoretical results obtained with the ten functionals combined with the triple-zeta basis set 6-311+G(2d,p) in a water medium and the experimental spectral data are presented in Table 3. The performance of the different functionals can be assessed by the mean absolute

deviations (MAD) of the theoretical values from the experiment. The MAD values for each of the functionals used are given in the last row of Table 3.

Table 3. The deviation from experiment of the theoretical vertical excitation energies (in eV) computed with different functionals combined with the 6-311+G(2d,p) basis set in a water medium for a series of cyanine dyes.

Dye	B3LYP	PBE0	M062X	BH&HLYP	CAM B3LYP	M06	M06L	HFS	HFB	B97D
TO	0.24	0.30	0.39	0.52	0.42	0.27	0.20	0.01	0.02	0.06
1b	0.25	0.31	0.40	0.54	0.44	0.29	0.21	0.01	0.04	0.06
B9	0.23	0.29	0.39	0.52	0.43	0.26	0.16	−0.03	−0.01	0.03
B11	0.23	0.29	0.38	0.52	0.42	0.26	0.16	−0.03	−0.01	0.03
B13	0.22	0.28	0.38	0.52	0.42	0.25	0.16	−0.06	−0.03	0.01
6b	0.11	0.17	0.33	0.41	0.35	0.15	0.07	−0.11	−0.09	−0.07
7Cl−TO	0.24	0.31	0.39	0.52	0.42	0.28	0.19	0.00	0.02	0.05
sof-5	0.19	0.26	0.39	0.51	0.43	0.23	0.04	−0.17	−0.13	−0.11
MAD [a]	0.21	0.28	0.38	0.51	0.42	0.25	0.15	−0.05	−0.02	0.01

[a] Mean absolute deviation from the experiment (*MAD*) $MAD = \frac{\sum|\lambda_{calc}-\lambda_{exp}|}{n}$, n–number of compounds.

All of the DFT functionals follow the experimental tendencies (Figure 3) and qualitatively describe the changes in the absorption maximum in the studied series. Such correlation between the experiment and theory indicates that the entire group of functionals is good enough for picturing the trends in the series.

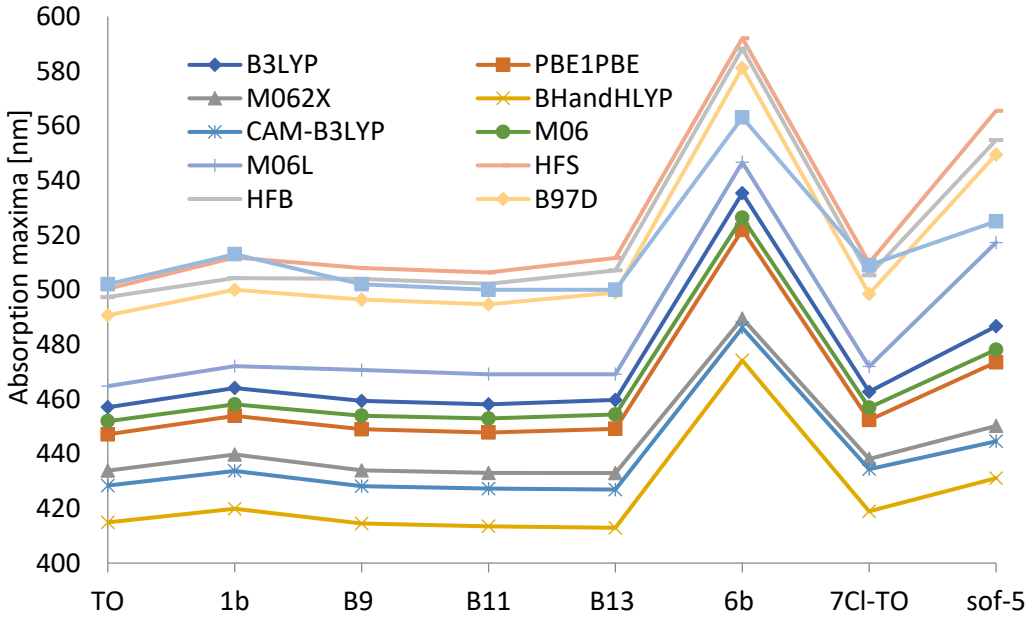


Figure 3. Trends in changes of the theoretical TDDFT vertical excitation energies (in nm) computed with different functionals combined with the 6-311+G(2d,p) basis set in a water medium and experimental absorption maxima from spectra in TE buffer for the series of cyanine dyes.

The deviation in the theoretically calculated absorption energies from the experimentally observed values for the electronic transitions (in eV) can be seen in Figure 4. It can be seen from Table 3 and Figure 4 that the hybrid functionals B3LYP, PBE0, and M06 (25–27% Hartree–Fock exchange) performed adequately for this class of dyes and can be used as a tool for calculating the electronic structures of monomethine cyanine dyes. Although they overestimate the transition energies, MAD is in the admissible range of 0.2–0.3 eV. The performance of the range-separated functional CAM-B3LYP is the worst in

our case, although it has been recommended for the calculation of electronic charge transfer transitions [65,67,68].

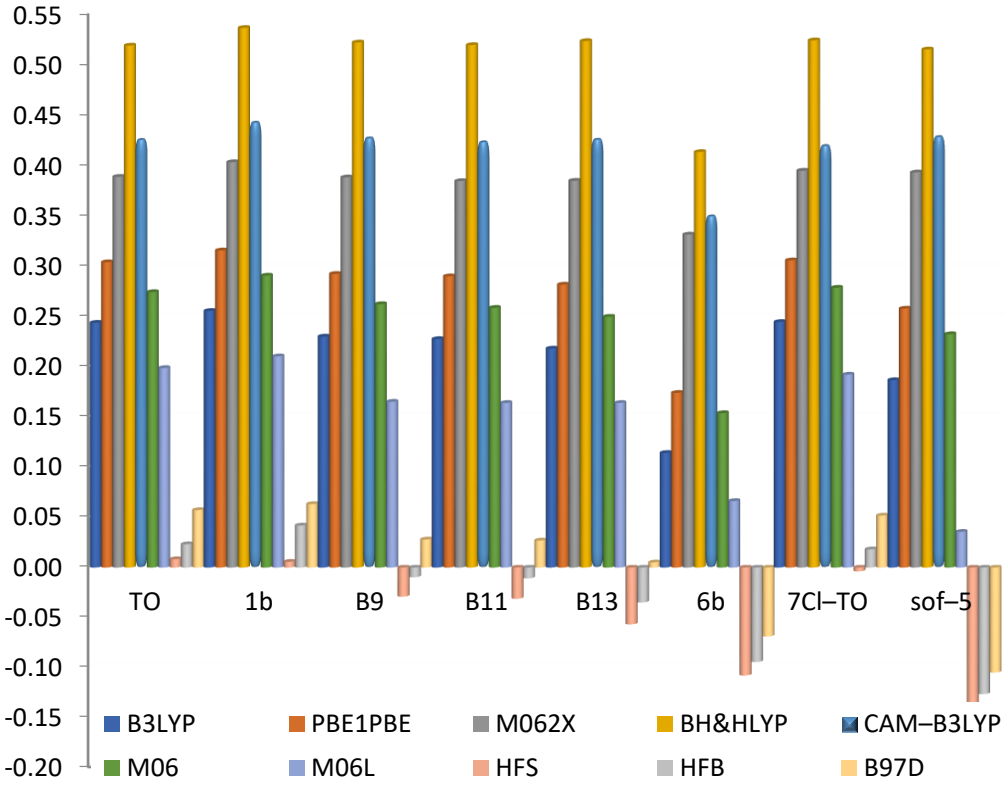


Figure 4. Deviations in the theoretical TDDFT vertical excitation energies (in eV) computed with different functionals combined with 6-311+G(2d,p) basis set in a water medium from the experimental data from spectra in TE buffer for the series of cyanine dyes.

In Gaussian 16, HFS stands for the Slater exchange. HFB is Becke's 1988 functional, which includes the Slater exchange with corrections involving the gradient of the density. The pure exchange functionals (M06L, HFS, HFB, B97D) show the best performance for the case study. All of these functionals have excellent performance and good predictability, the best being B97D with MAD 0.01 eV.

Based on these studies, we recommend that pure DFT functionals (M06L, HFS, HFB, B97D) be used to calculate the absorption properties of cyanine dyes.

3.3. Fluorescence

As mentioned earlier, the fluorescent response of cyanine dyes is sensitive to the environment. TO and its analogs have almost no fluorescence in organic solvents and exhibit a serious enhancement in the fluorescence intensity in viscous solutions (such as glycerin) and in DNA/RNA. The nature of fluorescence quenching in asymmetric cyanine dyes has been elucidated in several studies [66,69,70] and has been attributed to intramolecular torsion in the excited state. Easy rotation in solvent quenches the fluorescence. The fluorescence quantum yield increases when this rotation is obstructed. The geometry of the first TO excited state was optimized at B3LYP and PBE0 /6-311+G(2d,p) and is presented in Figure 5. The optimized ground-state geometry is planar, while the excited state is highly twisted. The vertical excitation leads to a locally excited state with a weak CT character (Figure 2) that has the same geometry as the ground state and has a planar structure. This local excited state has a transition energy of 2.51 eV (494nm). The optimization of the first excited state S_1 leads to a twisted geometry where the donor (quinolone moiety) and the acceptor (benzthiazole part) are perpendicular to each another (Figure 5). With the change in the dihedral angle between the two heterocycles (τ_2—Figure 6) a fully twisted dark state

is formed in accordance with previous findings [11–13]. This conformational changes in the structure of the fluorophore lead to the formation of a twisted intramolecular charge-transfer (TICT) excited state (S_1) [71]. The computed Stokes shift for TO is 1613 cm^{-1}, which agrees with the experimentally measured 1193 cm^{-1}. The fluorescence computations at B3LYP and PBE0 are in line with the experiment although the transition energies are slightly overestimated.

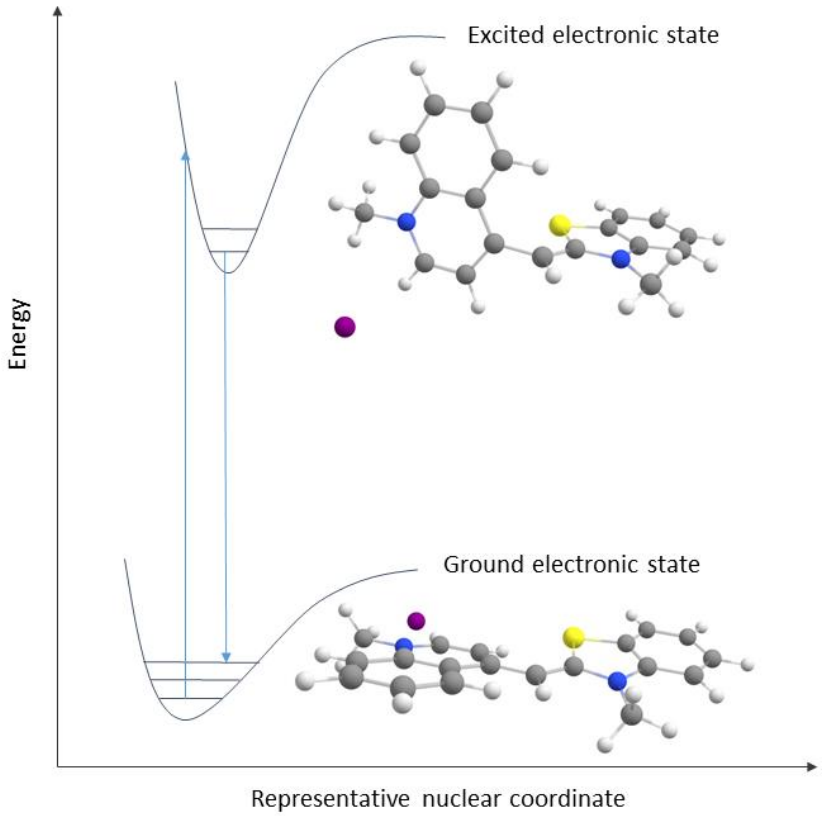


Figure 5. Schematic representation for ground (S_0) and excited state (S_1) geometries of TO.

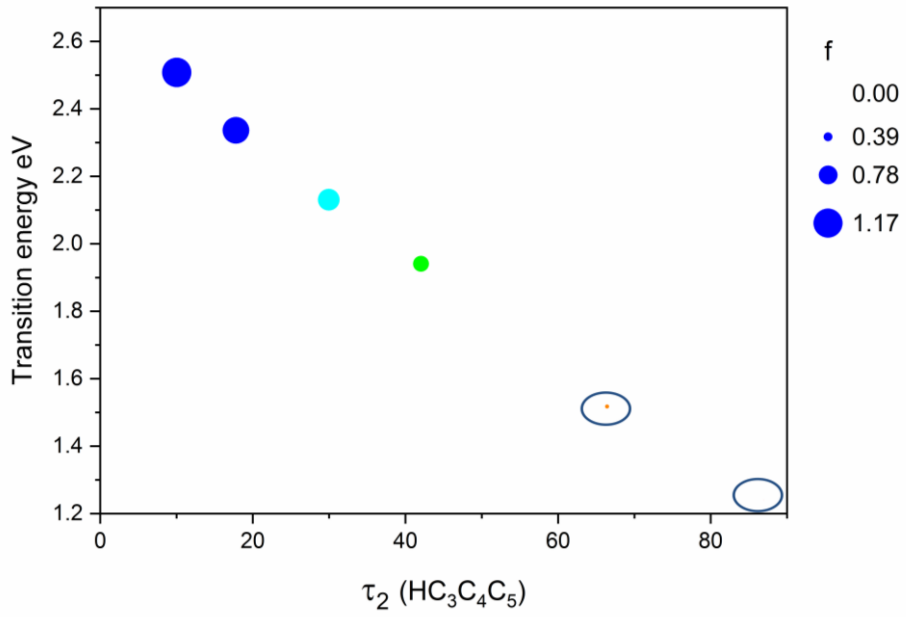


Figure 6. Excitation energies of TO as a function of the interplanar angle $\tau_2(HC_3C_4C_5)$. The radius of the circles is proportional to the predicted oscillator strength.

The conformational change in the excited state and the fact that the fluorescence intensity changes after binding of the dye to NA, thus leading to the fixation of the planar geometry, are the origin of the TO sensing mechanism and its analogs.

3.4. Aggregation of the Dyes

Monomethine cyanine dyes tend to aggregate in aqueous solution due to hydrophobic interactions. It has been suggested that the hydrophobicity and polarizability of dyes favor π-stacking interactions [72]. The self-aggregation of both TO and Benzthiazole Orange dyes has been found to occur but with deferent strength and other features depending on the dye itself [73]. An additional absorption band at 471 nm is observed in the absorption spectrum of TO alongside the dye's intrinsic absorption at 501 nm [73–75]. The band at 501 nm prevails at low concentrations, while at higher concentrations, the band at 471 predominates. This behavior is associated with the self-aggregation of the dye molecules and the formation of H dimers [74]. H-dimers are formed by interactions between the heterocyclic systems of two dye molecules located one above the other (the molecules are superimposed), while in the case of J dimers, molecule slipping relative to each other is observed. To address this behavior, we modeled four different π-stacked TO H-dimers, and their optimized geometry is shown in Figure 7.

During TO dimer optimization, the main challenge is maintaining π-stacking. The use of global hybrids such as B3LYP and PBE0 is not possible since the structure of the dimers falls apart during optimization. The dimer structures were optimized using the M062x functional. The presence of the iodide counterions was explicitly considered when modelling the structures. Mooi and Heyne [76] studied the effect of various counterions on aggregation. Counterions have been shown to play a significant role in terms of structural dimer organization and specific ionic effects.

The Gibbs free energy resulting from dimer formation was calculated at M062X/6-31G(d,p) from the following reaction: $2TO \rightarrow (TO)_2$. The optimized geometries of the H-dimers are shown in Figure 7, and the theoretical estimations are provided in Table 4. The most stable H-dimer is Dimer 2, where the donor part of the first molecule is above the acceptor part of the second TO molecule. The calculated Gibbs free energy resulting from the formation of the most stable dimer is −6.10 kcal/mol.

$K_D$has been experimentally measured in two different TO dimerization studies, with the following results being achieved: $-3.1 \times 10^4\ M^{-1}$ from [73] and $2.5 \times 10^4\ M^{-1}$ [77]. The Gibbs free energy of formation of the dimers was computed from the experiment using the equation ΔG= −RTlnK. The respective values were −6.12 kcal/mol and −6.00 kcal/mol. Thus, a very good agreement between the experiment and theory (−6.10 kcal/mol) was obtained in the present study.

The predicted vertical absorption values for the dimers are blue shifted according to the monomer absorption. The absorption maxima of the lowest energy TO dimer (Dimer 2) were calculated with HFS and HFB functionals determined to be the most accurate for the monomer absorption prediction. The obtained theoretical values are provided in Table 5. As seen from the table, the absorption maxima computed with HFB and HFS functionals are in very good agreement with the experimental values [73,75]. For comparison, the PBE0-calculated values are also provided in the table.

Dimer formation can be used as a model for the aggregation characteristics of TO analogs as well as analysis of the change in the fluorescence of the dye after binding to DNA. It can be stated that aggregation-induced fluorescence is observed during the dye aggregation process and upon dye-binding to NA.

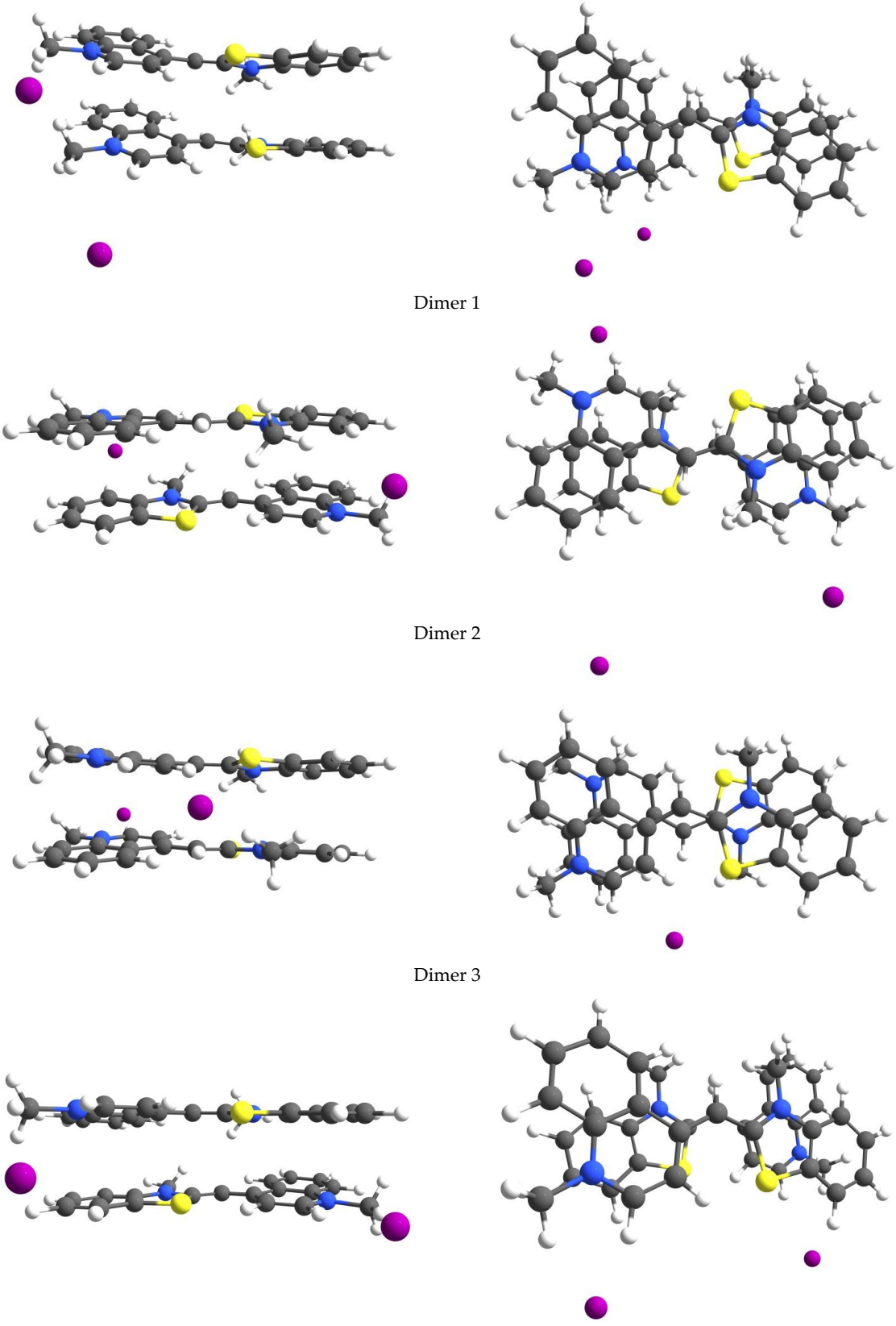


Figure 7. M062X/6-31G(d,p)-optimized molecular structures of TO H-dimers in water: left-top view, right-site view.

Table 4. M062X/6-31G(d,p) computed Gibbs free energy of formation (in kcal/mol) and absorption maxima (nm) of TO H-dimers.

TO Dimer	ΔG (kcal/mol)	λ_{abs} (nm) [a]
Dimer 1	−1.4	415
Dimer 2	−6.1	423
Dimer 3	−5.9	417
Dimer 4	−4.6	426

[a] From PBE0/6-311+G(2d,p) computations.

Table 5. Calculated absorption maxima (nm) for TO monomer and dimer.

Method/Basis Set	Monomer	Dimer
HFS/6-311+G(2d,p)	500	484
HFB/6-311+G(2d,p)	497	477
PBE0/6-311+G(2d,p)	447	423
experiment	501	471

4. Conclusions

A series of eight asymmetric cyanine dyes was modelled using DFT and TDDFT calculations. The calibration of the theoretical model for performing computational studies for dye molecules containing a particular chromophore was performed by examining the accuracy of ten functionals and six Pople-type basis sets. Theoretical results were validated against the experimental data. It was shown that the addition of one diffuse function to the 6-31G(d,p) basis set instantly increased the value of the calculated absorption maximum, thus improving the results obtained with 6-31+G(d,p). The large triple-zeta basis set 6-311+G(2d,p) showed the best performance. The comparison between the theoretical results obtained with the ten functionals combined with the triple-zeta basis set in a water medium and the experimental spectral data evince that the pure exchange functionals M06L, HFS, HFB, and B97D had the best performance in the case study.

Author Contributions: Conceptualization, S.I. and D.C.; methodology, S.I. and D.C.; validation, S.I., A.V., M.K. and D.C.; formal analysis, S.I. and D.C.; investigation, D.C.; resources, S.I.; data curation, S.I. and D.C.; writing—original draft preparation, S.I. and D.C.; writing—review and editing, S.I. and D.C.; visualization, D.C.; supervision, S.I. and D.C.; project administration, S.I. and D.C.; funding acquisition, S.I. All authors have read and agreed to the published version of the manuscript.

Funding: This research was funded by the BULGARIAN NATIONAL SCIENCE FUND (BNSF), grant number KP-06-H39/11 from 09.12.2019–SOFIa.

Acknowledgments: This work was supported by the Bulgarian National Science Fund (BNSF) project SOFIa (KP-06-H39/11), granted on 9 December 2019.

Conflicts of Interest: The authors declare no conflict of interest.

References

1. Pindur, U.; Jansen, M.; Lemster, T. Advances in DNA-Ligands with Groove Binding, Intercalating and/or Alkylating Activity: Chemistry, DNA-Binding and Biology. *Curr. Med. Chem.* **2005**, *12*, 2805–2847. [CrossRef] [PubMed]
2. Rask-Andersen, M.; Almén, M.S.; Schiöth, H.B. Trends in the exploitation of novel drug targets. *Nat. Rev. Drug Discov.* **2011**, *10*, 579–590. [CrossRef] [PubMed]
3. Saarnio, V.K.; Salorinne, K.; Ruokolainen, V.P.; Nilsson, J.R.; Tero, T.-R.; Oikarinen, S.; Wilhelmsson, L.M.; Lahtinen, T.M.; Marjomäki, V.S. Development of functionalized SYBR green II related cyanine dyes for viral RNA detection. *Dye. Pigment.* **2020**, *177*, 108282. [CrossRef]
4. Johnson, I.; Spence, M.T.Z. *The Molecular Probes Handbook—A Guide to Fluorescent Probes and Labeling Technologies*, 11th ed.; Life Technologies Corporation: Carlsbad, CA, USA, 2010.
5. Spielmann, H.P.; Wemmer, D.E.; Jacobsen, J.P. Solution Structure of a DNA Complex with the Fluorescent Bis-Intercalator TOTO Determined by NMR Spectroscopy. *Biochemistry* **1995**, *34*, 8542–8553. [CrossRef] [PubMed]
6. Yarmoluk, S.M.; Lukashov, S.S.; Ogul'Chansky, T.Y.; Losytskyy, M.Y.; Kornyushyna, O.S. Interaction of cyanine dyes with nucleic acids. XXI. Arguments for half-intercalation model of interaction. *Biopolymers* **2001**, *62*, 219–227. [CrossRef] [PubMed]

7. Zhytniakivska, O.; Girych, M.; Trusova, V.; Gorbenko, G.; Vasilev, A.; Kandinska, M.; Kurutos, A.; Baluschev, S.B. Spectroscopic and molecular docking studies of the interactions of monomeric unsymmetrical polycationic fluorochromes with DNA and RNA. *Dye. Pigment.* **2020**, *180*, 108446. [CrossRef]
8. Ziarani, G.M.; Moradi, R.; Lashgari, N.; Kruger, H.G. Cyanine Dyes. In *Metal-Free Synthetic Organic Dyes*; Elsevier: Amsterdam, The Netherlands, 2018; pp. 127–152. [CrossRef]
9. Armitage, B.A. Cyanine dye-DNA interactions: Intercalation, groove binding, and aggregation. In *DNA Binders and Related Subjects*; Waring, M.J., Chaires, J.B., Eds.; Springer: Berlin/Heidelberg, Germany, 2005; Volume 253, pp. 55–76. ISBN 3540228357.
10. Mishra, A.; Behera, R.K.; Behera, P.K.; Mishra, B.K.; Behera, G.B. Cyanines during the 1990s: A Review. *Chem. Rev.* **2000**, *100*, 1973–2012. [CrossRef]
11. Silva, G.L.; Ediz, V.; Yaron, D.; Armitage, B.A. Experimental and Computational Investigation of Unsymmetrical Cyanine Dyes: Understanding Torsionally Responsive Fluorogenic Dyes. *J. Am. Chem. Soc.* **2007**, *129*, 5710–5718. [CrossRef]
12. Rastede, E.E.; Tanha, M.; Yaron, D.; Watkins, S.C.; Waggoner, A.S.; Armitage, B.A. Spectral fine tuning of cyanine dyes: Electron donor–acceptor substituted analogues of thiazole orange. *Photochem. Photobiol. Sci.* **2015**, *14*, 1703–1712. [CrossRef]
13. Biancardi, A.; Biver, T.; Marini, A.; Mennucci, B.; Secco, F. Thiazole orange (TO) as a light-switch probe: A combined quantum-mechanical and spectroscopic study. *Phys. Chem. Chem. Phys.* **2011**, *13*, 12595–12602. [CrossRef]
14. Jacquemin, D.; Zhao, Y.; Valero, R.; Adamo, C.; Ciofini, I.; Truhlar, D.G. Verdict: Time-Dependent Density Functional Theory "Not Guilty" of Large Errors for Cyanines. *J. Chem. Theory Comput.* **2012**, *8*, 1255–1259. [CrossRef] [PubMed]
15. Vus, K.; Girych, M.; Trusova, V.; Gorbenko, G.; Kurutos, A.; Vasilev, A.; Gadjev, N.; Deligeorgiev, T. Cyanine dyes derived inhibition of insulin fibrillization. *J. Mol. Liq.* **2019**, *276*, 541–552. [CrossRef]
16. Gorbenko, G.; Trusova, V.; Kirilova, E.; Kirilov, G.; Kalnina, I.; Vasilev, A.; Kaloyanova, S.; Deligeorgiev, T. New fluorescent probes for detection and characterization of amyloid fibrils. *Chem. Phys. Lett.* **2010**, *495*, 275–279. [CrossRef]
17. Vasilev, A.; Deligeorgiev, T.; Kaloyanova, S.; Stoyanov, S.; Maximova, V.; Vaquero, J.J.; Alvarez-Builla, J. Synthesis of novel tetracationic asymmetric monomeric monomethine cyanine dyes—Highly fluorescent dsDNA probes. *Color. Technol.* **2011**, *127*, 69–74. [CrossRef]
18. Kandinska, M.; Cheshmedzhieva, D.; Kostadinov, A.; Rusinov, K.; Rangelov, M.; Todorova, N.; Ilieva, S.; Ivanov, D.; Videva, V.; Lozanov, V.; et al. Tricationic asymmetric monomeric monomethine cyanine dyes with chlorine and trifluoromethyl functionality—Fluorogenic nucleic acids probes. *J. Mol. Liq.* **2021**, *342*, 117501. [CrossRef]
19. Sato, Y. Design of Fluorescent Peptide Nucleic Acid Probes Carrying Cyanine Dyes for Targeting Double-Stranded RNAs for Analytical Applications. *Bull. Chem. Soc. Jpn.* **2020**, *93*, 406–413. [CrossRef]
20. Martineau, C.; Whyte, L.G.; Greer, C.W. Development of a SYBR safe™ technique for the sensitive detection of DNA in cesium chloride density gradients for stable isotope probing assays. *J. Microbiol. Methods* **2008**, *73*, 199–202. [CrossRef]
21. Gibson, J.F.; Kelso, S.; Skevington, J.H. Band-cutting no more: A method for the isolation and purification of target PCR bands from multiplex PCR products using new technology. *Mol. Phylogenetics Evol.* **2010**, *56*, 1126–1128. [CrossRef]
22. Clauß, M.; Springorum, A.C.; Hartung, J. Comparison of Different Fluorescence and Non-Fluorescence Staining Techniques for Rapid Detection of Airborne Micro-Organisms Collected on Room Temperature Vulcanizing (RTV) Silicones from Generated Aerosols and from Ambient Air. *Aerosol Sci. Technol.* **2012**, *46*, 818–827. [CrossRef]
23. Pérez-Cordero, J.-J.; Sánchez-Suárez, J.; Delgado, G. Use of a fluorescent stain for evaluating in vitro infection with Leishmania panamensis. *Exp. Parasitol.* **2011**, *129*, 31–35. [CrossRef]
24. Send, R.; Valsson, O.; Filippi, C. Electronic Excitations of Simple Cyanine Dyes: Reconciling Density Functional and Wave Function Methods. *J. Chem. Theory Comput.* **2011**, *7*, 444–455. [CrossRef] [PubMed]
25. Charaf-Eddin, A.; Le Guennic, B.; Jacquemin, D. Excited-states of BODIPY–cyanines: Ultimate TD-DFT challenges? *RSC Adv.* **2014**, *4*, 49449–49456. [CrossRef]
26. Grimme, S.; Neese, F. Double-hybrid density functional theory for excited electronic states of molecules. *J. Chem. Phys.* **2007**, *127*, 154116. [CrossRef] [PubMed]
27. Zhekova, H.; Krykunov, M.; Autschbach, J.; Ziegler, T. Applications of Time Dependent and Time Independent Density Functional Theory to the First π to π^* Transition in Cyanine Dyes. *J. Chem. Theory Comput.* **2014**, *10*, 3299–3307. [CrossRef]
28. Le Guennic, B.; Jacquemin, D. Taking Up the Cyanine Challenge with Quantum Tools. *Acc. Chem. Res.* **2015**, *48*, 530–537. [CrossRef]
29. Koch, W.; Holthausen, M.C. *A Chemist's Guide to Density Functional Theory*; John Wiley & Sons: Hoboken, NJ, USA, 2001.
30. Cheshmedzhieva, D.; Ivanova, P.; Stoyanov, S.; Tasheva, D.; Dimitrova, M.; Ivanov, I.; Ilieva, S. Experimental and theoretical study on the absorption and fluorescence properties of substituted aryl hydrazones of 1,8-naphthalimide. *Phys. Chem. Chem. Phys.* **2011**, *13*, 18530–18538. [CrossRef]
31. Jacquemin, D.; Wathelet, V.; Perpète, E.A.; Adamo, C. Extensive TD-DFT Benchmark: Singlet-Excited States of Organic Molecules. *J. Chem. Theory Comput.* **2009**, *5*, 2420–2435. [CrossRef]
32. Jacquemin, D.; Perpète, E.A.; Ciofini, I.; Adamo, C.; Valero, R.; Zhao, Y.; Truhlar, D. On the Performances of the M06 Family of Density Functionals for Electronic Excitation Energies. *J. Chem. Theory Comput.* **2010**, *6*, 2071–2085. [CrossRef]
33. Jacquemin, D.; Perpète, E.A.; Scalmani, G.; Frisch, M.J.; Kobayashi, R.; Adamo, C. Assessment of the efficiency of long-range corrected functionals for some properties of large compounds. *J. Chem. Phys.* **2007**, *126*, 144105. [CrossRef]

34. Roos, B.O.; Fülscher, M.; Malmqvist, P.-Å.; Merchán, M.; Serrano-Andrés, L. Theoretical Studies of the Electronic Spectra of Organic Molecules. In *Quantum Mechanical Electronic Structure Calculations with Chemical Accuracy*; Springer: Dordrecht, The Netherlands, 1995; pp. 357–438.
35. Truhlar, D.G. Valence bond theory for chemical dynamics. *J. Comput. Chem.* **2007**, *28*, 73–86. [CrossRef]
36. Champagne, B.; Guillaume, M.; Zutterman, F. TDDFT investigation of the optical properties of cyanine dyes. *Chem. Phys. Lett.* **2006**, *425*, 105–109. [CrossRef]
37. Frisch, M.J.; Trucks, G.W.; Schlegel, H.B.; Scuseria, G.E.; Robb, M.A.; Cheeseman, J.R.; Scalmani, G.; Barone, V.; Petersson, G.A.; Nakatsuji, H.; et al. *Gaussian 16 Revision 16.A.03*; Gaussian, Inc.: Wallingford, CT, USA, 2016.
38. Labanowski, J.K.; Andzelm, J.W. (Eds.) *Density Functional Methods in Chemistry*; Springer: New York, NY, USA, 1991; ISBN 978-1-4612-7809-2.
39. Petersson, G.A.; Bennett, A.; Tensfeldt, T.G.; Al-Laham, M.A.; Shirley, W.A.; Mantzaris, J. A complete basis set model chemistry. I. The total energies of closed-shell atoms and hydrides of the first-row elements. *J. Chem. Phys.* **1988**, *89*, 2193–2218. [CrossRef]
40. Nazeeruddin, M.K.; De Angelis, F.; Fantacci, S.; Selloni, A.; Viscardi, G.; Liska, P.; Ito, S.; Takeru, B.; Grätzel, M. Combined Experimental and DFT-TDDFT Computational Study of Photoelectrochemical Cell Ruthenium Sensitizers. *J. Am. Chem. Soc.* **2005**, *127*, 16835–16847. [CrossRef] [PubMed]
41. Asaduzzaman, A.M.; Schreckenbach, G. Computational study of the ground state properties of iodine and polyiodide ions. *Theor. Chem. Acta* **2009**, *122*, 119–125. [CrossRef]
42. Lin, R.Y.-Y.; Chuang, T.-M.; Wu, F.-L.; Chen, P.-Y.; Chu, T.-C.; Ni, J.-S.; Fan, M.-S.; Lo, Y.-H.; Ho, K.-C.; Lin, J.T. Anthracene/Phenothiazine π-Conjugated Sensitizers for Dye-Sensitized Solar Cells using Redox Mediator in Organic and Water-based Solvents. *ChemSusChem* **2015**, *8*, 105–113. [CrossRef]
43. Sohrabi, M.; Amirnasr, M.; Farrokhpour, H.; Meghdadi, S. A single chemosensor with combined ionophore/fluorophore moieties acting as a fluorescent "Off-On" Zn^{2+} sensor and a colorimetric sensor for Cu^{2+}: Experimental, logic gate behavior and TD-DFT calculations. *Sens. Actuators B Chem.* **2017**, *250*, 647–658. [CrossRef]
44. Cossi, M.; Barone, V.; Cammi, R.; Tomasi, J. Ab initio study of solvated molecules: A new implementation of the polarizable continuum model. *Chem. Phys. Lett.* **1996**, *255*, 327–335. [CrossRef]
45. Tomasi, J.; Mennucci, B.; Cammi, R. Quantum Mechanical Continuum Solvation Models. *Chem. Rev.* **2005**, *105*, 2999–3094. [CrossRef]
46. Becke, A.D. Density-functional thermochemistry. IV. A new dynamical correlation functional and implications for exact-exchange mixing. *J. Chem. Phys.* **1996**, *104*, 1040–1046. [CrossRef]
47. Perdew, J.P.; Ernzerhof, M.; Burke, K. Rationale for mixing exact exchange with density functional approximations. *J. Chem. Phys.* **1996**, *105*, 9982–9985. [CrossRef]
48. Adamo, C.; Barone, V. Toward reliable adiabatic connection models free from adjustable parameters. *Chem. Phys. Lett.* **1997**, *274*, 242–250. [CrossRef]
49. Zhao, Y.; Truhlar, D.G. The M06 suite of density functionals for main group thermochemistry, thermochemical kinetics, noncovalent interactions, excited states, and transition elements: Two new functionals and systematic testing of four M06-class functionals and 12 other functionals. *Theor. Chem. Acc.* **2008**, *120*, 215–241. [CrossRef]
50. Becke, A.D. A new mixing of Hartree-Fock and local density-functional theories. *J. Chem. Phys.* **1993**, *98*, 1372–1377. [CrossRef]
51. Yanai, T.; Tew, D.; Handy, N.C. A new hybrid exchange–correlation functional using the Coulomb-attenuating method (CAM-B3LYP). *Chem. Phys. Lett.* **2004**, *393*, 51–57. [CrossRef]
52. Hohenberg, P.; Kohn, W. Inhomogeneous Electron Gas. *Phys. Rev.* **1964**, *136*, B864–B871. [CrossRef]
53. Kohn, W.; Sham, L.J. Self-consistent equations including exchange and correlation effects. *Phys. Rev.* **1965**, *140*, A1133–A1138. [CrossRef]
54. Becke, A.D. Density-functional exchange-energy approximation with correct asymptotic behavior. *Phys. Rev. A* **1988**, *38*, 3098–3100. [CrossRef]
55. Grimme, S. Semiempirical GGA-type density functional constructed with a long-range dispersion correction. *J. Comput. Chem.* **2006**, *27*, 1787–1799. [CrossRef]
56. Krishnan, R.; Binkley, J.S.; Seeger, R.; Pople, J.A. Self-consistent molecular orbital methods. XX. A basis set for correlated wave functions. *J. Chem. Phys.* **1980**, *72*, 650–654. [CrossRef]
57. Kaloyanova, S.; Ivanova, I.; Tchorbanov, A.; Dimitrova, P.; Deligeorgiev, T. Synthesis of chloro-substituted analogs of Thiazole orange—Fluorophores for flow cytometric analyses. *J. Photochem. Photobiol. B Biol.* **2011**, *103*, 215–221. [CrossRef]
58. Vasilev, A.A.; Kandinska, M.I.; Stoyanov, S.S.; Yordanova, S.B.; Sucunza, D.; Vaquero, J.J.; Castaño, O.D.; Baluschev, S.; Angelova, S.E. Halogen-containing thiazole orange analogues—New fluorogenic DNA stains. *Beilstein J. Org. Chem.* **2017**, *13*, 2902–2914. [CrossRef] [PubMed]
59. Evenson, W.E.; Boden, L.M.; Muzikar, K.A.; O'Leary, D.J. 1H and 13C NMR Assignments for the Cyanine Dyes SYBR Safe and Thiazole Orange. *J. Org. Chem.* **2012**, *77*, 10967–10971. [CrossRef] [PubMed]
60. Runge, E.; Gross, E. Density-Functional Theory for Time-Dependent Systems. *Phys. Rev. Lett.* **1984**, *52*, 997–1000. [CrossRef]
61. Casida, M.E. Time-Dependent Density Functional Response Theory for Molecules. In *Recent Advances in Density Functional Methods*; Recent Advances in Computational Chemistry; World Scientific: Singapore, 1995; pp. 155–192. [CrossRef]

62. Jacquemin, D.; Mennucci, B.; Adamo, C. Excited-state calculations with TD-DFT: From benchmarks to simulations in complex environments. *Phys. Chem. Chem. Phys.* **2011**, *13*, 16987–16998. [CrossRef]
63. Toulouse, J.; Colonna, F.; Savin, A. Long-range–short-range separation of the electron-electron interaction in density-functional theory. *Phys. Rev. A* **2004**, *70*, 062505. [CrossRef]
64. Seminario, J.M. (Ed.) *Recent Developments and Applications of Modern Density Functional Theory*; Elsevier: Amsterdam, The Netherlands, 1996; pp. 327–354. ISBN 9780444824042.
65. Oberhofer, K.E.; Musheghyan, M.; Wegscheider, S.; Wörle, M.; Iglev, E.D.; Nikolova, R.D.; Kienberger, R.; Pekov, P.S.; Iglev, H. Individual control of singlet lifetime and triplet yield in halogen-substituted coumarin derivatives. *RSC Adv.* **2020**, *10*, 27096–27102. [CrossRef]
66. Hunt, P.A.; Robb, M.A. Systematic Control of Photochemistry: The Dynamics of Photoisomerization of a Model Cyanine Dye. *J. Am. Chem. Soc.* **2005**, *127*, 5720–5726. [CrossRef]
67. Yang, D.; Liu, Y.; Shi, D.; Sun, J. Theoretical study on the excited-state photoinduced electron transfer facilitated by hydrogen bonding strengthening in the C337–AN/MAN complexes. *Comput. Theor. Chem.* **2012**, *984*, 76–84. [CrossRef]
68. Pedone, A. Role of Solvent on Charge Transfer in 7-Aminocoumarin Dyes: New Hints from TD-CAM-B3LYP and State Specific PCM Calculations. *J. Chem. Theory Comput.* **2013**, *9*, 4087–4096. [CrossRef]
69. Karunakaran, V.; Lustres, J.L.P.; Zhao, L.; Ernsting, N.P.; Seitz, O. Large Dynamic Stokes Shift of DNA Intercalation Dye Thiazole Orange has Contribution from a High-Frequency Mode. *J. Am. Chem. Soc.* **2006**, *128*, 2954–2962. [CrossRef]
70. Sanchez-Galvez, A.; Hunt, P.; Robb, M.A.; Olivucci, M.; Vreven, A.T.; Schlegel§, H.B. Ultrafast Radiationless Deactivation of Organic Dyes: Evidence for a Two-State Two-Mode Pathway in Polymethine Cyanines. *J. Am. Chem. Soc.* **2000**, *122*, 2911–2924. [CrossRef]
71. Retting, W. Charge Separation in Excited States of Decoupled Systems—TICT Compounds and Implications Regarding the Development of New Laser Dyes and the Primary Process of Vision and Photosynthesis. *Angew. Chem. Int. Ed. Engl.* **1986**, *25*, 971–988. [CrossRef]
72. West, W.; Pearce, S. The Dimeric State of Cyanine Dyes. *J. Phys. Chem.* **1965**, *69*, 1894–1903. [CrossRef]
73. Biver, T.; Boggioni, A.; Secco, F.; Turriani, E.; Venturini, M.; Yarmoluk, S. Influence of cyanine dye structure on self-aggregation and interaction with nucleic acids: A kinetic approach to TO and BO binding. *Arch. Biochem. Biophys.* **2007**, *465*, 90–100. [CrossRef]
74. Ogul'Chansky, T.; Losytskyy, M.; Kovalska, V.; Yashchuk, V.; Yarmoluk, S. Interactions of cyanine dyes with nucleic acids. XXIV. Aggregation of monomethine cyanine dyes in presence of DNA and its manifestation in absorption and fluorescence spectra. *Spectrochim. Acta Part A Mol. Biomol. Spectrosc.* **2001**, *57*, 1525–1532. [CrossRef]
75. Nygren, J.; Svanvik, N.; Kubista, M. The interactions between the fluorescent dye thiazole orange and DNA. *Biopolymers* **1998**, *46*, 39–51. [CrossRef]
76. Mooi, S.M.; Heyne, B. Size Does Matter: How To Control Organization of Organic Dyes in Aqueous Environment Using Specific Ion Effects. *Langmuir* **2012**, *28*, 16524–16530. [CrossRef]
77. Mooi, S.M.; Keller, S.N.; Heyne, B. Forcing Aggregation of Cyanine Dyes with Salts: A Fine Line between Dimers and Higher Ordered Aggregates. *Langmuir* **2014**, *30*, 9654–9662. [CrossRef]